10.1109/ULTSYM.2014.0605

Improving the quality of attenuation imaging using full angular spatial compounding

Omar Zenteno[1], Adam Luchies[2], Michael Oelze[2] and Roberto Lavarello[1]
[1]Laboratorio de Imágenes Médicas, Departamento de Ingeniería
Pontificia Universidad Católica del Perú, San Miguel, Lima 32, Perú.
[2] Bioacoustics Research Laboratory, Department of Electrical and Computer Engineering
University of Illinois at Urbana-Champaign, Urbana, IL 61801, USA.

***Abstract*—The quantitative imaging of attenuation coefficients slope (ACS) has the potential to improve medical diagnostics. However, attempts to characterize ACS using pulse-echo data have been limited by the large statistical variations in the estimates. Previous studies demonstrated that it is possible to extend the trade-off between variance and spatial resolution of quantitative ultrasound, spectral-based parameters by the use of full angular (i.e., 360◦) spatial compounding (FASC). In the present work, the use of FASC has been extended to the estimation of ACS and its performance has been experimentally evaluated using two physical phantoms. The ACSs of the background and inclusion regions were estimated using insertion loss measurements to be 0.41 and 0.75 dB/cm/MHz for Phantom #1, and 0.54 and 1.04 dB/cm/MHz for Phantom #2, respectively. Pulse-echo data were collected using a 7.5 MHz, f/4 transducer at 30 angles of view uniformly distributed between 0 and 360º. Single view ACS maps were generated using a spectral log difference method with 0.6 by 0.6 mm data blocks. The FASC images were constructed by assigning to a pixel the median of its corresponding estimates from all 30 angles of view. The reduction in the variance of the FASC estimates compared to the variance of estimates from a single view (i.e., variance averaged from the 30 single views) in the inclusion and background regions were 89.18% and 88.71% for Phantom #1 and 92.33% and 86.98% for Phantom #2. Moreover, in all the cases the estimation bias in the inclusion and background regions using FASC was lower than 9.0%. These results suggest that the variance of attenuation coefficient slope estimation can be significantly reduced without sacrificing spatial resolution by the use of full angular spatial compounding.**

Keywords— Attenuation imaging, Tissue characterization, Spatial compounding.

I. Introduction

Common B-mode ultrasound imaging has been the first hand diagnosis tool on soft tissue pathologies for several years due to its low cost and portability. However, diagnostics from conventional ultrasound are always subjective and heavily dependent on the operator's experience, medical training and image quality. In addition, radiofrequency (RF) echoes contain extra information about the tissue properties that cannot be evaluated with the signal envelope approach only. One of these properties, which can provide important information for radiological diagnostics, is the ultrasonic attenuation coefficient.

Quantitative ultrasound attenuation coefficient estimates offer numerical depth- and frequency-dependent values based on the power spectrum of the RF data. Several studies show that specific pathological tissue has different attenuating properties when comparing to healthy tissues. The attenuation coefficient slope (ACS), combined with other statistical parameters and tissue properties (i.e., image texture, backscatter coefficients), has been used to diagnose diffuse liver diseases [1, 2] and characterize breast tissues [3]. Attenuation coefficients have been proposed as potential tools for predicting cervical ripening in rats [4] and humans [5]. The possibility to differentiate between Graves' and Hashimoto's thyroid disease based on ACS estimates has been explored [6]. In addition, the accurate estimation of attenuation coefficients has been shown to be a determining factor on the precision of similar parameter estimation, e.g., backscatter coefficients (BSC) [7].

However, estimated attenuation coefficients have been characterized by their high level of variance due to coherent scattering. Currently, ACS images are constructed using large data blocks in order to reduce the variance of the resulting attenuation maps. Few authors have made use of the coherence reduction benefits of multiple sample compounding when measuring QUS parameters [8, 9]. A recent study in particular shows that the QUS-BSC imaging with compounding can achieve optimal performance with samples of an object from 360 degree views [10]. The present study complements these findings to assess the feasibility of reducing statistical errors in attenuation estimation images using an analytical diffraction compensation function.

II. Methods

A. QUS analytic attenuation estimation method

Several frequency domain attenuation estimation algorithms have been reviewed in the literature (e.g., spectral and spectral log difference [11], hybrid method [11, 12], and spectral cross correlation [13], among others). All these methods require a frequency- and depth-dependent diffraction compensation factor to account for spectral losses. The majority of the previously mentioned algorithms make use of a calibrated reference phantom to compensate for diffraction. In contrast, in this work the analytic attenuation estimation method for single-element transducers presented in [14] has been used.

The spectral information of RF data was processed to generate attenuation maps on custom MATLAB (MathWorks, Natick, MA) software. Several regions of interest were outlined in the phantoms and data blocks of 0.6mm by 0.6mm with an 87.5% overlap in both directions were used to window the data. Each group of lines inside a data block was divided into two shorter blocks, proximal and distal, determined by the size of the gating function as shown in Fig. 1. For each block, a Tukey window with α= 0.25 was used as gating function.

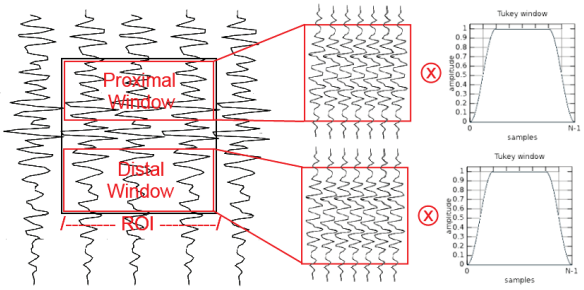

Fig. 1. Data block and gate function distribution over the sample. Data blocks were overlaid to increase spatial resolution of the attenuation maps.

As shown in [14], the resulting attenuation coefficient slope for each region of interest can be obtained by performing a linear fit to (1),

$$\alpha(\omega)+\frac{\ln[c]}{4\cdot(r_d-r_p)}=\frac{1}{4\cdot(r_d-r_p)}\cdot\ln\left[\frac{\left\langle|V_s(r_p,\omega)|^2\right\rangle}{\langle|V_s(r_d,\omega)|^2\rangle}\cdot\frac{D_s(r_d,\omega)}{D_s(r_p,\omega)}\right], \quad (1)$$

where r is the distance from the transducer to the center of the window of analysis, subscripts d and p represent the distal and proximal window of the data block respectively, $V_s(r,\omega)$ is the received voltage signal from the scattering volume, $D_s(r,\omega)$ is the analytical BSC diffraction compensation function for single-element transducers proposed by [15] and c is a constant term product of assuming that BSC varies in the form $\eta(r_p,\omega)=c\cdot\eta(r_p,\omega)$.

Finally, the attenuation coefficient slope β in dB/cm-MHz can be calculated as

$$\beta = 8.6858\gamma, \quad (2)$$

where γ is the linear fit slope of (1).

B. *Full angular spatial compounding (FASC)*

Spatial compounding has demonstrated efficacy for reducing speckle and improving contrast in B-mode images. The principle behind spatial compounding is that the speckle pattern changes depending on the insonification source relative position to the scattering region. Therefore, different position and angular sampling averaging can reduce the variance of the resulting image.

The proposed approach consists of obtaining RF data from each ROI at different angles, as shown in Fig. 2. A single element transducer is translated laterally over the sample, capturing adjacent RF lines. Once the complete target has been acquired, another set of RF lines is captured, this time from a different angular plane to the target. The procedure is repeated until a 360º view sample has been completed. This method allows capturing more RF measurements corresponding to the same ROI without the need to increase its size.

The complete single view RF data set is processed to generate corresponding attenuation coefficient maps. Each attenuation coefficient map is automatically segmented based on the B-mode image brightness level to remove low signal to noise ratio (SNR) areas, then is registered to relocate each pixel corresponding to the same spatial location. Finally the compounding image was constructed by calculating the pixel-wise median value considering all single views. Therefore, the variance of the QUS estimates can be reduced without degrading the spatial resolution.

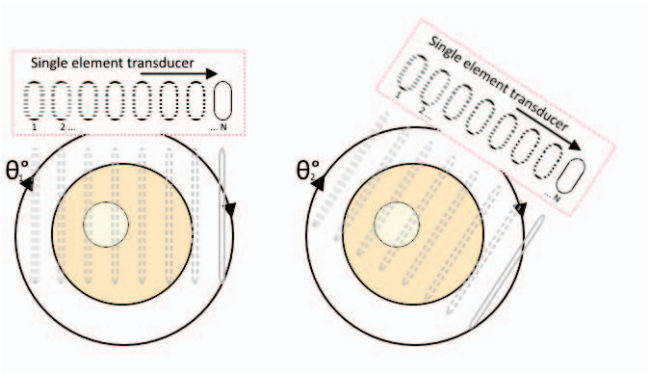

Fig. 2. Proposed full angular spatial compounding configuration. A single element transducer is moved laterally to create an N multi-linear data sample of the target. Process is repeated over a full angular stepped trajectory of 360º

C. *Sample preparation and data acquisition*

The sample group consisted of two agar-based phantoms. Each phantom was formed in the shape of a cylinder consisting of a 70 mm diameter background region with an eccentric 20 mm diameter inclusion. Powdered graphite was mixed with the agar in order to modify the attenuation coefficient in the background and inclusion regions.

Pulse-echo data were collected using a 7.5 MHz weakly-focused (f/4) single element transducer and an Olympus Panametrics 5900 pulser/receiver (Olympus NDT, Waltham, MA) for excitation. The RF data were captured by a PC using a 14-bit UF3-4121 A/D card with 250 MHz sampling frequency (Strategic Test Corporation, Woburn, MA).

Each agar phantom was scanned using a micro-positioning system controlled by custom LabVIEW (National Instruments, Austin, TX) software. 30 angular samples were taken at a step of 12º around the phantom's circular peripheral wall. The attenuation coefficient slopes of the background and inclusion regions were independently estimated using insertion loss measurements, and were found to be 0.41 and 0.75 dB/cm/MHz for Phantom #1, and 0.54 and 1.04 dB/cm/MHz for Phantom #2, respectively.

D. *Statistics*

For statistics, manual segmentation of the data blocks that were fully included on each area of the phantoms (i.e., background and inclusion) was performed using custom MATLAB software. The mean and variance of attenuation

estimates from single views were compared to views from full angular compounding. The estimation mean percentage error (MPE) and the variance reduction rate (VRR) were computed in percentile values as shown in (3) and (4) respectively:

$$MPE = \frac{100\%}{n} \cdot \sum_{i=1}^{n} \frac{s_i - v}{v}, \quad (3)$$

where s_i is i-th view mean attenuation value of the area of analysis and v is the corresponding attenuation measurement obtained with the insertion loss test.

$$VRR = 100\% \cdot \left(1 - \frac{\sigma_0^2}{\sigma_1^2}\right), \quad (4)$$

where $\sigma_0^2$is the mean variance of all the single view estimates included on the area of analysis and σ_1^2 the corresponding variance of the FASC estimates.

III. Experimental Results

Examples of the B-mode images obtained from single view of both phantoms are shown on the first row of Fig. 3. The inclusion areas exhibit a higher echogenicity than their corresponding background regions. However, no quantitative information is available from these images. The corresponding single view attenuation coefficient images are shown in the second row of Fig. 3. Even though the geometry of the phantoms is roughly described in these images, the large variance in the images reduces the visualization of the circular inclusions. Moreover, there is not enough quantitative information at certain depths due the low SNR and bandwidth loss caused by the attenuation of the backscattered signal. Finally, the full angular spatial compounding attenuation maps for both phantoms are shown in the third row of Fig. 3. Both attenuation images accurately described the spatial position of the inclusions present on the physical phantoms. In addition, an attenuation coefficient slope map of the whole phantom and a reduction in the estimation bias was achieved.

TABLE I. Percentile estimation error and variance reduction

Area		Single view MPE	FASC percentile error	VRR
Phantom #1	Background	9.24%	4.88%	88.71%
	Inclusion	14.52%	6.67%	88.33%
Phantom #2	Background	3.55%	1.85%	89.18%
	Inclusion	14.37%	7.69%	88.06%

Table 1 presents the attenuation coefficient slope errors for both single view and FASC images, and the variance reduction obtained when using multiple view rather than single view data. The estimated values using FASC of the background and inclusion regions were 0.39 and 0.70 dB/cm/MHz for Phantom #1, and 0.53 and 0.96 dB/cm/MHz for Phantom #2, respectively. Therefore, the estimated mean values obtained with FASC were consistent with the ones obtained with the insertion loss method. In addition, the use of full angular spatial compounding resulted in an average variance reduction of 88% considering the background and inclusion areas in both phantoms.

IV. Discussion

In both cases a significant VRR was achieved. Although a similar MPE performance was expected for single view and FASC estimates, lower MPE were achieved with the latter. In both cases, the MPE of inclusion and background regions using FASC was lower than 8.0% and the VRR higher than 88%. In addition, a moderate improvement in estimation bias was observed. This improvement may be due to the nonlinear processing (i.e., median calculation) used to construct the FASC images.

The single view QUS attenuation maps had some areas which did not contain information due to SNR and bandwidth loss over depth. The use of multifocal beamforming or coded excitation enhancement techniques, like resolution enhancement compression, may be of great use to remove these single-view depth limitations. Increasing the robustness of the single-view estimates could lead to an increment in FASC performance.

The variance improvement obtained in this study was similar to the one observed in [10] when estimating BSCs using FASC. The high level of accuracy and precision in the results suggests that the joint estimation of backscatter and attenuation coefficient using FASC is promising. Moreover, these methods have the potential to be implemented on ultrasound medical scanners capable of full angular coverage (i.e., ultrasound breast tomography [16]).

V. Conclusion

The results presented in this work suggest that the variance and field of view of attenuation coefficient slope imaging can be significantly improved without sacrificing spatial resolution by the use of full angular spatial compounding.

Acknowledgment

This work was supported by NIH Grant R01 EB008992 and PUCP Grant DGI 70242-2149

References

[1] Z. F. Lu, J. Zagzebski, and F. Lee, “Ultrasound backscatter and attenuation in human liver with diffuse disease,” *Ultrasound in Medicine & Biology*, vol. 25, no.7, pp. 1047–1054, 1999.

[2] G. Goutam, R. Lavarello, J. P. Kemmerer, R. Miller, and M. L. Oelze. "Ex vivo study of quantitative ultrasound parameters in fatty rabbit livers," Ultrasound in medicine & biology, vol. 38, no. 12, pp 2238-2248,2012.

[3] F. D'Astous and F. Foster, “Frequency dependence of ultrasound attenuation and backscatter in breast tissue,” *Ultrasound in Medicine & Biology*, vol. 12, no.1, pp.795-808, 1986.

[4] B. L. McFarlin, W. D. O’Brien, Jr., M. L. Oelze, J. F. Zachary, and R. C. White-Traut, “Quantitative ultrasound assessment of the rat cervix,” *Journal of Ultrasound in Medicine*, vol. 25, no. 8, pp. 1031–1040, 2006

[5] Y. Labyed, T. A. Bigelow, and B. L. Mcfarlin, “Estimate of the attenuation coefficient using a clinical array transducer for the detection of cervical ripening in human pregnancy,” *Ultrasonics*, vol 51, no. 1, pp. 34–39, 2011

[6] Y. Fuji, N. Taniguchi, K. Itoh, K. Omoto, “Attenuation coefficient measurement in the thyroid,” *Journal of Ultrasound in Medicine*, vol 22, no.10, pp. 1067-1073, 2003

[7] T. A. Bigelow. and W. D. O'Brien, Jr., "Impact of local attenuation approximations when estimating correlation length from backcattered ultrasound echoes," *Journal of the Acoustical Society of America*, vol 120, no.1, pp. 546-553, 2006.

[8] A. Gerig, T. Varghese and J. Zagzebski, "Improved parametric imaging of scatterer size estimates using angular compounding," *IEEE Transactions on Ultrasonics, Ferroelectrics and Frequency Control*, vol. 51, no. 6, pp. 708 – 715, 2004.

[9] Z. Klimonda, J. Litniewski, P. Karwat, W. Secomski and A.Nowicki, "Tissue attenuation imaging – Synthetic aperture focusing versus spatial compounding," *in Proceedings of the IEEE International Ultrasonics Sympsium*, pp. 2360-2363, 2012.

[10] R. Lavarello, J. Sanchez and M. Oelze, "Improving the quality of QUS imaging using full angular spatial compounding," *in Proceedings of the IEEE International Ultrasonics Sympsium*, pp. 32-35, 2008.

[11] Y. Labyed and T. Bigelow, "A theoretical comparison of attenuation measurement techniques from backscattered ultrasound echoes," *Journal of the Acoustical Society of America*, vol. 129, no. 4, pp. 2316-2324, 2011.

[12] H. Kim and T. Varghese, "Hybrid spectral domain method for attenuation slope estimation," *Ultrasound in Medicine & Biology*, vol. 34, no.11, pp. 1808–1819, 2008.

[13] H. Kim and T. Varghese, "Attenuation estimation using spectral cross-correlation," *IEEE Transactions on Ultrasonics, Ferroelectrics and Frequency Control*, vol. 54, no. 3, pp.510-520, 2007.

[14] O. Zenteno, W. Ridgway, S. Sarwate, M. Oelze and R. Lavarello, "Ultrasonic attenuation imaging in a rodent thyroid cancer model," *in Proceedings of the IEEE International Ultrasonics Symposium*, pp. 88-91, 2013.

[15] X. Chen, D. Phillips, K. Schwarz, J. Mottley, and K. Parker, "The measurement of backscatter coefficient from a broadband pulse-echo system: a new formulation," *IEEE Transactions on Ultrasonics, Ferroelectrics and Frequency Control*, vol. 44, no. 2, pp. 515–525, 1997.

[16] R. Lavarello, M. Oelze, M. Berggren, S. Johnson, M. Orescanin and R. Yapp, "Implementation of scatterer size imaging on an ultrasonic breast tomography scanner," *in Proceedings of the IEEE International Ultrasonics Sympsium*, pp. 305-308, 2009.

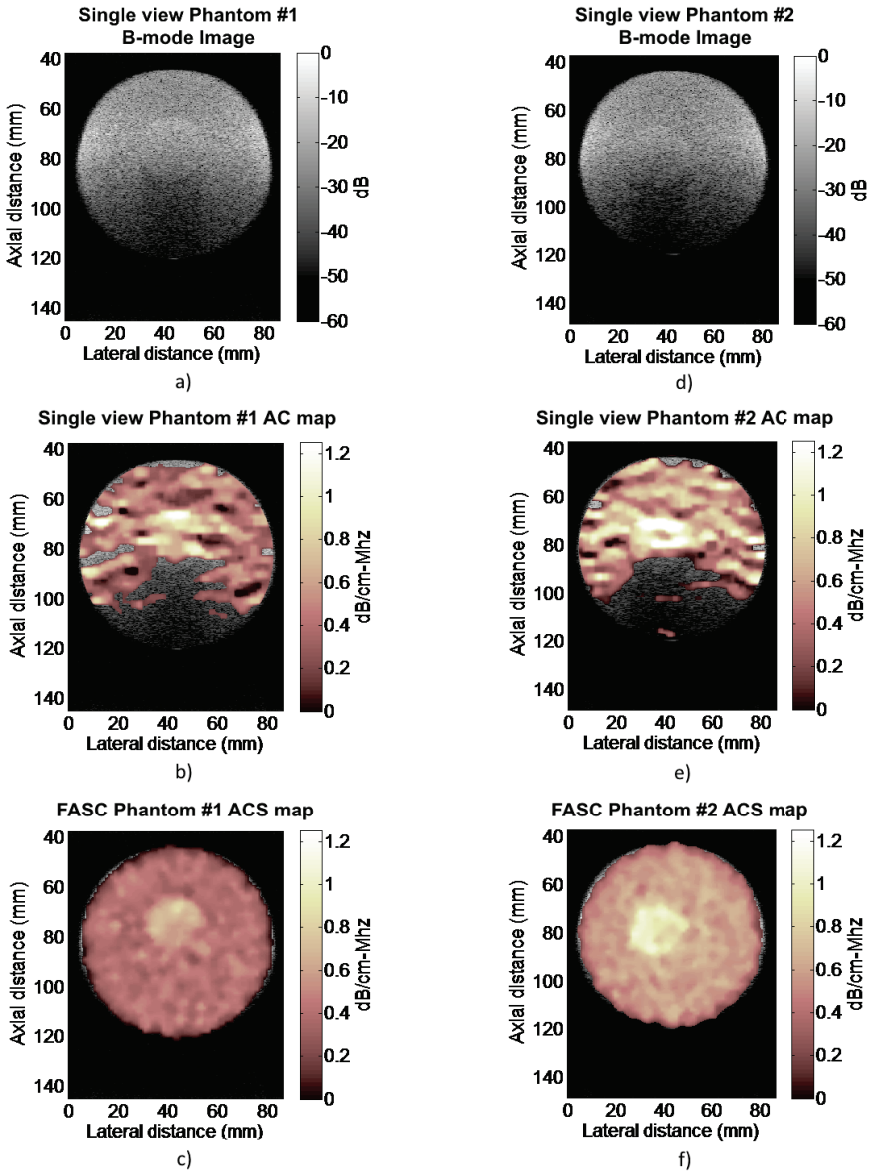

Fig. 3. (a),(d), Examples of the B-mode images obtained from single view of both phantoms. (b),(e), Corresponding single view attenuation coefficient images. (c),(f) Full angular spatial compounding attenuation maps for both phantoms.